hexagon, and 60-gon) as a function of the driving voltage position (i.e., MM zone number). Note that the coupling coefficients for the respective geometries are almost identically the same. The top curve represents the values for the triangular loop. The lowest curve (solid) is the value for the 60-gon (circular) loop. The other polygonal loops fall in between these values uniformly as a function of the number of sides in the polygon. Obviously, the specific number of sides of the regular polygonal loop has very little effect on the coupling coefficients for the fundamental (first harmonic) natural modes. However, at higher harmonic frequencies, significant differences in the coupling coefficients for the various shapes can be seen. It is apparent from these plots, that driving a polygonal loop antenna at certain specific positions (i.e., MM zone position #15, #30, and #45) on the loop periphery produces current distributions which may be completely devoid of certain modal distributions. Likewise, driving the loop at other specific positions, allows the designer to choose just how much of each of the fundamental (orthogonal) modes of a certain frequency he may desire for adjusting the loop antenna resonant frequency or the input impedance.

IV. Conclusion

A singularity expansion method analysis has been carried out on planar, thin-wire, regular polygonal loop antennas. Specifically, the SEM parameters: natural frequencies, natural modes, and coupling coefficients, have been determined numerically for the equilateral triangle, the square, the pentagon, the hexagon, and the 60-gon (circle). Particular attention was focused on determining the specific conditions which produce "splitting" of the otherwise degenerate natural frequencies associated with the rotationally orthogonal natural modes. Enhanced coupling to these loop antennas results when the driving excitation is positioned specifically to excite the mode (or modes) associated with one (or more) of these "split" natural frequencies. The results obtained and presented offer new insights into the fundamental electromagnetic nature of thin-wire polygonal loop antennas.

While it is apparent that the authors have probably generated a significant number of questions that have not been answered completely by the data and associated discussion presented here, it is believed that other interested investigators, if made aware of these findings, might be stimulated by these ruminations to consider other antenna and scattering problems from this interesting perspective.

References

[1] R. W. P. King, "Theory of the corner-driven square loop antenna," *IRE Trans. Antennas Propagat.*, vol. AP-4, pp. 393-407, 1956.

[2] P. A. Kennedy, "Loop antenna measurements," *IRE Trans. Antennas Propagat.*, vol. AP-4, pp. 610-618, 1956.

[3] E. Storer, "Impedance of thin-wire loop antennas," *AIEE Trans.*, vol. 75, p. 606, 1956.

[4] T. Tsukiji and S. Tou, "On polygonal loop antennas," *IEEE Trans. Antennas Propagat.*, vol. AP-28, pp. 571-575, 1980.

[5] R. F. Blackburn and D. R. Wilton, "Analysis and synthesis of an impedance-loaded loop antenna using the singularity expansion method," *IEEE Trans. Antennas Propagat.*, vol. AP-26, pp. 136-140, 1978.

[6] E. J. Rothwell and N. Gharsallah, "Determination of the natural frequencies of a thin wire elliptical loop," *IEEE Trans. Antennas Propagat.*, vol. AP-35, pp. 1319-1324, 1987.

[7] R. F. Harrington, *Field Computation by Moment Methods*. New York: Macmillan, 1968.

[8] C. E. Baum, "The singularity expansion method," in *Topics in Applied Physics*, vol. 10: *Transient Electromagnetic Fields*. L. B. Felsen, Ed. New York: Springer-Verlag, 1976.

Phase Centers of Horn Antennas Using Gaussian Beam Mode Analysis

JOHN A. MURPHY, MEMBER, IEEE, AND
RACHAEL PADMAN, MEMBER, IEEE

Abstract—**The power of Gaussian beam mode analysis to describe accurately the propagation of electromagnetic beams and the location of a horn antenna phase-center is illustrated. By way of example, the case of a compensated pyramidal horn fitted with fins to produce a less abruptly tapered E-plane field distribution is discussed and the results obtained are compared with those from an alternative method published in the literature. Excellent agreement is found.**

I. Introduction

This work arose from the need to know the phase center position of the centimeter-wave horn antennas used as feeds on the Cassegrain reflector dishes of the Mullard Radio Astronomy Observatory 5 km-aperture synthesis telescope [1]. The telescope is in the process of being upgraded; as part of the process we are reexamining the coupling of the feed horns to the individual dishes. An accurate description of the feed beam patterns and location of the phase centers is necessary to ensure correct positioning of the feeds.

The telescope operates at frequencies of 2.7, 5, and 15 GHz. The subreflector is in the *near field* of the feed at 2.7 GHz, while it is in the *far field* at 15 GHz. One of the advantages of the Gaussian mode beam analysis is that it is equivalent to the Fresnel description of diffraction, and so gives an accurate beam amplitude and phase profile in *both* the near field and the far field, for systems with moderate focal ratios ($F > 2$) [2].

The phase center of the horn can be defined as the center of curvature of the intersection of the far-field equiphase surface with a plane containing the horn axis [3]. However, there is nothing special about the far-field (Fraunhofer) region, and it is often important to consider the near-field Fresnel region as well [4], [5]. This is because the phase center position depends on the distance from the horn aperture of the plane perpendicular to the axis across which one measures the phase [5]. In the case of a long horn with a focal ratio $F > 2$, for example, the phase center measured on a plane near the horn aperture appears to be at the horn apex (since the radius of curvature of the phase front in the aperture is given by the slant length of the horn), while in the far field the phase center appears to be near the horn aperture.

Analytical approaches to determining the phase center positions have been applied to some horn configurations, for example [3]-[5]. These usually involve integration of the fields over the horn aperture to determine the near-field or far-field phase behavior of the radiation fields. If one can express the equiphase surface directly in terms of the off-axis angle, then the phase center can be determined by using some method to calculate the radius of curvature of the phase front [3], [5]. Another approach, which is similar to the method described in this communication, involves plotting the phase in the far field [6].

An alternative to aperture integration for calculating the amplitude and phase evolution of a propagating beam of radiation uses Gaussian beam mode analysis. In this approach the field at the aperture of

Manuscript received March 22, 1989; revised September 7, 1989.

J. A. Murphy is with the Department of Experimental Physics, Maynooth College, Kildare, Ireland.

R. Padman is with the Cavendish Laboratory, Madingley Road, Cambridge, CB3 0HE, UK.

IEEE Log Number 9036296.

the horn is *decomposed* into a sum of *beam modes* [7]. All these constituent beam modes have identical equiphase radii of curvature [8]. However, as the beam from the horn propagates, the relative phases of the modes also shift (according to a simple relationship), which results in the introduction of residual phase distortion in the horn beam with respect to the spherical phase front defined by the individual modes [9]. Thus, the position of the *horn beam* phase center will be determined by a combination of both phase curvature introduced by the residual phase distortion and the common radius of curvature for the individual propagating beam modes

The details of the Gaussian beam mode analysis approach are described in Sections II and III for the example case of the compensated pyramidal horns referred to above. Results exist in the literature [3] for this type of horn and we compare our results with those.

II. Hermite-Gaussian Beam Mode Expansion

The relevant dimensions of the horns are shown in Fig. 1. They are referred to as amplitude compensated horns [10], and have nonuniform aperture illumination along the E-plane, unlike the standard single-moded pyramidal horn. The field incident on the fin structure from the fundamentally moded rectangular waveguide will have the usual TE_{10} amplitude distribution. Because of its geometry, the fin structure affects the E-plane, but not the H-plane, amplitude distribution at the horn aperture. Since *power* must be conserved in the beam as it propagates in each of the three regions defined by the fins, the *amplitudes* of the fields at the horn mouths will be determined by the ratio of relative areas there compared to those at the other end of the fin structure. Thus, in this case, the amplitude of the E-field at the horn aperture will be uniform, but lower, in the outer two regions (1 and 3) than in the inner region 2 (see Fig. 2), giving a reduced far field sidelobe level in the E-plane.

The field at the horn aperture is given by [3]

$$E(x, y) = E_{0i} \cdot \cos(\pi x/a) \cdot \exp(-j\pi x^2/\lambda L_x - j\pi y^2/\lambda L_y) \quad (1)$$

where $E_{01} = E_{03} < E_{02}$ (the subscripts refer to the region) and L_x and L_y are the slant lengths in the x and y directions, respectively. The H-plane width of the horn aperture is a and λ is the wavelength of the radiation. These fields can be expanded as a sum of Hermite-Gaussian beam modes [11]:

$$E(x, y) = \sum_{m=0}^{m=\infty} \sum_{n=0}^{n=\infty} A_{mn}(W_x, W_y) \cdot \psi_{mn}(x/W_x, y/W_y) \cdot \exp(-\pi j/\lambda \cdot (x^2/R_x + y^2/R_y)) \quad (2)$$

where $\psi_{mn}(x/W_x, y/W_y) = (W_x \cdot W_y)^{-1/2} \cdot H_m(\sqrt{2}x/W_x) \cdot H_n(\sqrt{2}y/W_y) \cdot \exp(-x^2/W_x^2 - y^2/W_y^2)$. $H_m(\rho)$ is the Hermite polynomial of order m in ρ.

The choice of W_x and W_y, and R_x and R_y is *arbitrary*; however, in order to match the phase fronts at the horn aperture we set $R_x = L_x$, and $R_y = L_y$, which then implies that the A_{mn} are real. Thus, the equiphase radii of curvature are the same for the horn aperture fields as for *each* of the beam modes in the sum (with the center of curvature at the horn apex).

The values of W_x and W_y usually are chosen to maximize the power in the fundamental (0, 0) mode [7]. This fixes the positions of an E-plane and an H-plane "virtual waist" inside the horn, from which the *individual* beam mode components of the field appear to emanate. Ideally, the waist positions and radii should coincide for the two orthogonal planes, but this is true only in special cases [12]. The distance from the horn aperture to the virtual waist position is given by

$$\Delta_{x,y}(W_{x,y}) = L_{x,y}/(1 + (\lambda L_{x,y}/\pi W_{x,y}^2)^2). \quad (3)$$

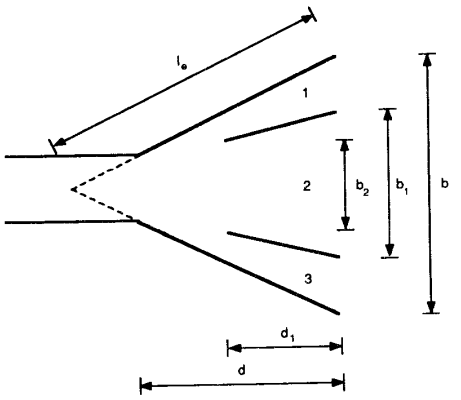

freq (GHz)	b (mm)	b_1 (mm)	b_2 (mm)	l_e (mm)	d (mm)	d_1 (mm)
2.7	380	188	166	1686	1525	708
5.0	217	105	91	1702	1525	713
15.0	73	35.5	31	386.4	343	169

Fig. 1. The E-plane horn dimensions.

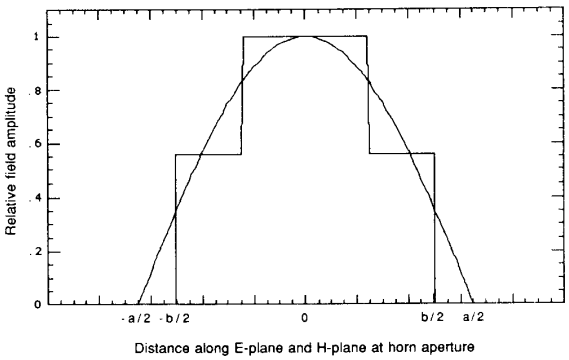

Fig. 2. E-field amplitudes at horn aperture.

As the beam propagates, $W_{x,y}$ and $R_{x,y}$ for the component Gaussian modes are functions of distance from the virtual waists, as described in [8] and [13]. A mode-number dependent *phase slippage* term φ_{mn} also appears in the expansion of the fields. If we assume the beam propagates along the positive z axis, with $z = 0$ at the horn aperture, the expansion for $E(x, y)$ at z is given by

$$E(x, y; z) = \sum_{m=0}^{m=\infty} \sum_{n=0}^{n=\infty} A_{mn}(W_x(0), W_y(0)) \cdot \psi_{mn}(x/W_x(z), y/W(z)) \times \exp(-\pi j/\lambda \cdot (x^2/R_x(z) + y^2/R_y(z)) + j(\varphi_{mn}(z))). \quad (4a)$$

The phase slippage term is given by

$$\varphi_{mn}(z) = \left(m + \frac{1}{2}\right) \cdot \varphi_{0x}(z) + \left(n + \frac{1}{2}\right) \cdot \varphi_{oy}(z) \quad (4b)$$

where

$$\varphi_{ox}(z) = [\tan^{-1}(\pi W_x^2(z)/\lambda R_x(z)) - \tan^{-1}(\pi W_x^2(0)/\lambda L)]$$

$$\varphi_{oy}(z) = [\tan^{-1}(\pi W_y^2(z)/\lambda R y(z)) - \tan^{-1}(\pi W_y^2(0)/\lambda L)].$$

$W_x(0)$ and $W_y(0)$ refer to values chosen at the horn aperture. One can easily show that the radii of curvature $R_{x,y}$ (as a function of z) are given by

$$R_{x,y}(z) = (z + \Delta_{x,y}) + (\lambda L_{x,y}/\pi W_{x,y}^2(0))^2 \cdot (\Delta_{x,y}^2/(z + \Delta_{x,y})). \tag{5}$$

Thus, in the Fresnel region the center of curvature does *not* coincide with the waist position.

At any point along the propagation axis, the phase front radii of curvature $R_{x,y}$ are the same for all the modes in the expansion. Nevertheless these $R_{x,y}$ may *not* be the best fit phase radii of curvature for the *sum* of the beam modes; relative to $R_{x,y}$ there may be some residual phase deviation due to the effect of the φ_{mn} terms. If this residual phase has a quadratic component in x (or y), then R_x (or R_y) is not equal to the best fit radius of curvature. The actual determination of this best fit radius is discussed in the next section.

III. Locating the Phase Centers

As already noted, at the aperture of the horn the choice of values for $W_x(0)$ and $W_y(0)$ is arbitrary. If we allow $W_x(0)$ (or $W_y(0)$) to vary, then there are three interesting consequences:

1) The position of the virtual waist shifts according to (3),
2) the radius of curvature $R_x(z)$ or $R_y(z)$ for the beam modes change according to (5), and
3) the curvature of the residual phase deviation changes since the A_{mn} and φ_{mn} are functions of the $W_x(0)$ and $W_y(0)$ as in (4a).

This provides a method for determining the position of the x- and y-plane phase centers. If we vary the values of $W_x(0)$ and $W_y(0)$ until the residual phases (after subtracting the calculated curvatures $R_{x,y}$), in the plane z = constant, each have zero curvature, then the corresponding $R_x(z)$ and $R_y(z)$ are equal to the *best approximations* to the phase curvatures *on axis*. To find the center of curvature relative to the horn, we estimate the distance Δ behind the aperture of the new virtual waist in each plane. The phase center is then located a distance d_p behind the horn aperture and is given by

$$d_p(W(0)) = [(z + L)/(z + \Delta(W(0))] \cdot \Delta(W(0)) \tag{6}$$

where the x, y suffixes are implied and Δ is the virtual waist displacement behind the horn aperture for $W(0)$, as given in (3). Thus, determining the phase center location can be regarded as a process in which we adjust the virtual waist position to set the curvature of the residual phase (as defined above) to zero.

An example of the effect on the E-plane phase of changing $W(0)$ for the 15 GHz horn is shown in Figs. 3(a) and 3(b). In Fig. 3(a) the deviation of the phase from a wavefront with radius of curvature R is evaluated at a distance of 1600 mm from the horn aperture for various values of $W(0)$, the approximate position of the subreflector. At such a distance from the horn a 10 dB edge taper corresponds to a subreflector of radius 400 mm. The value of $W(0)$ that gives the most uniform *average* phase over the relevant region is chosen by inspection—for this case it is in the range of 26–28 mm (see Fig. 3(a)). For a larger diameter subreflector a larger value for the optimum $W(0)$ will be found, as is clear from Fig. 3(a). This procedure could clearly be automated if so desired.

However, the phase center is usually defined such that the residual

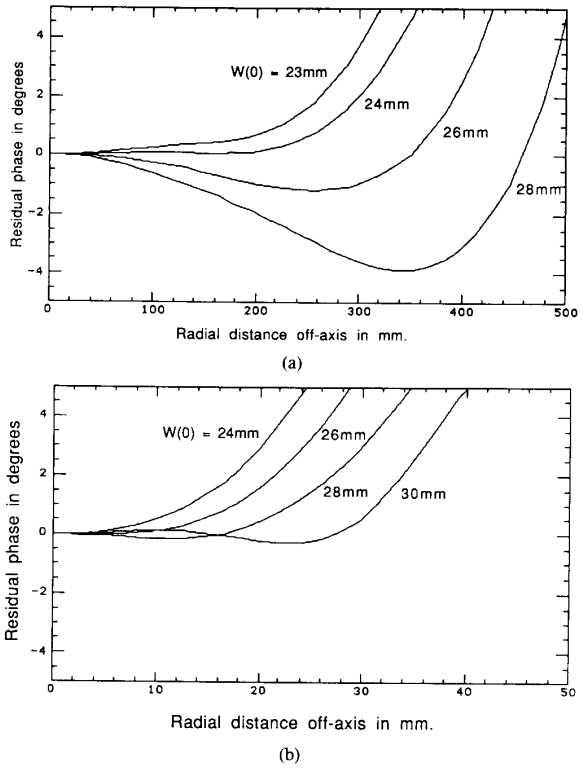

Fig. 3. (a) Effect of changing $W(0)$ at horn aperture on the residual phase for subreflector-horn separation of 1600 mm (far-field case). (b) Effect of changing $W(0)$ at horn aperture on residual phase for subreflector-horn separation of 160 mm (near-field case).

phase deviation has zero curvature *on the horn axis*. In that case a value of $W(0) \approx 24$ mm yields the least on-axis curvature at a distance z of 1600 mm (almost in the far field). For this value of $W(0)$, the distance of the phase center behind the horn aperture d_p, given by (6), is 24 mm. For the true far-field case, it is again found that $W(0) \approx 24$ mm; however, because $R \gg \Delta$, d_p decreases to 20 mm. We also consider the hypothetical near-field example case of a subreflector 160 mm from the horn aperture. As can be seen in Fig. 3(b), $W(0) \approx 30$ mm yields least phase distortion, corresponding to a d_p of 57 mm.

Results are published in the literature [3] for the far-field case of a compensated horn where the amplitude ratio along the E-plane is 1 : 2 : 1, and where $b_1 = b/2$ (b and b_1 as defined in Fig. 1). For such an amplitude compensated horn of slant length 368.4 mm and b of 73 mm, the predicted value for d_p from [3, Fig. 4] equals 19 mm. The Gaussian beam analysis approach yields a value for d_p in the far field of 18.5 mm, which, especially given that $\lambda = 20$ mm, agrees well. To compare the Gaussian beam analysis approach with that presented in [3] over a wider range of horn apertures and lengths, we examined some specific examples: $b/\lambda = 8, l/\lambda = 70$, and $b/\lambda = 5$, $l/\lambda = 10$, both of which correspond to a $d_p = 5.5\lambda$ using [3, Fig. 4]. The results produced by the Gaussian analysis approach for these two cases are: $d_p = (6.1 \pm 1.0)\lambda$ and $d_p = (5.9 \pm 1.0)\lambda$, respectively, where $\pm 1.0\lambda$ represents the phase depth of field. Clearly, there is excellent agreement between the two approaches.

If we wanted to optimize the *aperture efficiency*, we would then need to evaluate the coupling integral between the horn beam pattern at the subreflector and the illumination pattern due to a distant point source on the antenna boresight for various horn/subreflector

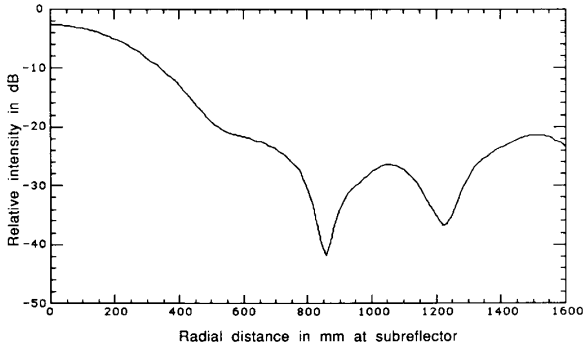

Fig. 4. Calculated E-plane beam pattern at the subreflector for 15 GHz horn.

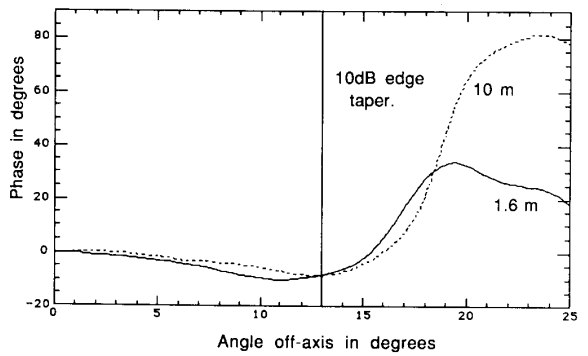

Fig. 5. Near-field (1.6 m from horn) and far-field (10 m from horn) effects on calculated phase variation in the E-plane for a fixed value of W at horn aperture (5 GHz horn with $W(0) = 92$ mm, optimized for maximum power in the fundamental mode.)

separations. The calculated amplitude distribution is independent of $W(0)$ if sufficiently many modes are included in the sum: the E-plane distribution (using 40 modes) is shown in Fig. 4.

We also show, in Fig. 5, the effect on the residual phase in the case of the 5 GHz horn for horn/subreflector separations of 1.6 and 10.0 m, where $W(0) = 92$ mm (beam width optimised for maximum power in the fundamental mode). The beam E-plane profiles are shown in Fig. 6. The effects of diffraction between the near- and far-field profiles are clearly visible.

In summary, the use of Gaussian beam mode analysis as an alternative method for estimating the phase center of a horn has a number of advantages.

1) It allows one to follow the near-field and the far-field phase behavior of the horn beam.

2) The phase center can conveniently be expressed in terms of the virtual waist position inside the horn by adjusting *one* parameter $W(0)$ in the modal expansion of the field at the mouth of the horn.

3) Since the method involves plotting the phase over the plane of interest, it is possible to determine whether the residual phase distortion *off-axis* should be considered as, for example, when one is trying to optimise aperture efficiency.

4) The approach also enables one to determine the phase "depth of field" in terms of positioning of the horn, as there may be no appreciable residual phase curvature for a range of $W(0)$ and thus a range of waist positions.

5) In horn-fed antenna systems involving quasi-optical components [12] such as lenses or focussing mirrors, the Gaussian beam

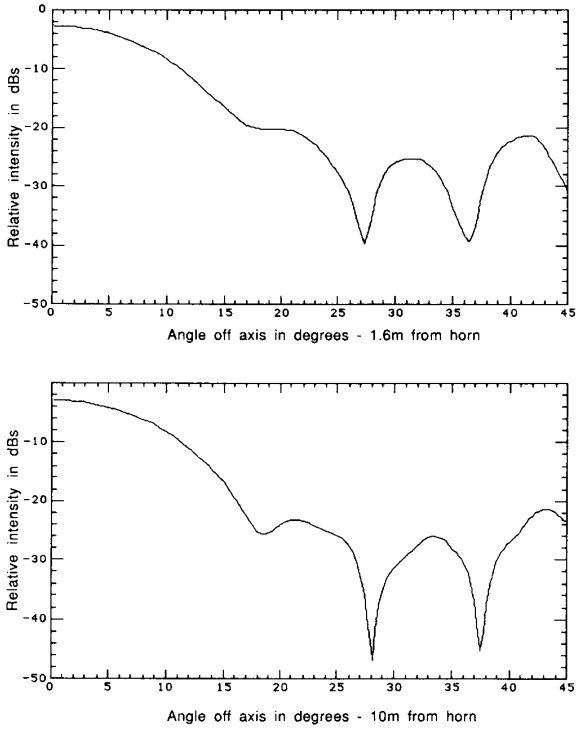

Fig. 6. Calculated beam patterns in the E-plane of 5 GHz horn 1.6 and 10 m from horn aperture.

formalism conveniently allows one to reconstruct the feed pattern in amplitude and phase exactly at the antenna, and thus determine the horn "phase center" for such a system [2].

6) The Gaussian beam analysis approach is extremely efficient. Calculation of the (real) modal coefficients just involves a straightforward *equiphase* surface integration at the horn aperture (no phase variation need be taken into account). The beam phase variation can then be readily reconstructed anywhere in the near field, as well as in the far field, using the already calculated mode coefficients.

Acknowledgment

The authors thank Richard Saunders and Guy Pooley for suggesting the problem addressed in this work. The referee's comments were very useful.

References

[1] M. Ryle, "Radio telescopes of large resolving power," *Sci.*, vol. 188, pp. 1071, 1975.

[2] R. Padman, J. A. Murphy, and R. E. Hills, "Gaussian mode analysis of Cassegrain antenna efficiency," *IEEE Trans. Antennas Propagat.*, vol. AP-35, pp. 1093–1103, 1987.

[3] E. I. Muehldorf, "The phase center of horn antennas," *IEEE Trans. Antennas Propagat.*, vol. AP-18, pp. 753–760, 1970.

[4] E. R. Nagelberg, "Fresnel region phase centers of circular aperture antennas," *IEEE Trans. Antennas Propagat.*, vol. AP-13, pp. 479–480, 1965.

[5] I. Ohtera and H. Ujie, "Nomographs for phase centers of conical corrugated and TE_{11} mode horns," *IEEE Trans. Antennas Propagat.*, vol. AP-23, pp. 858–859, 1975.

[6] Y. Y. Hu, "A method of determining phase centers and its application to electromagnetic horns," *J. Franklin Inst.*, pp. 31–39, 1961.

[7] R. J. Wylde, "Millimetre-wave gaussian beam mode optics and corrugated feed horns," *Proc. Inst. Elec. Eng.*, vol. 131, pt. H, pp. 258–262, 1984.

[8] H. Kogelnik and T. Li, "Laser beams and resonators," *Proc. IEEE*, vol. 54, pp. 1312–1325, Oct. 1966.
[9] J. A. Murphy, "Aperture efficiencies of large axis-symmetric reflector antennas fed by conical horns," *IEEE Trans. Antennas Propagat.*, vol. AP-36, pp. 570–575, 1988.
[10] G. M. Peace and E. E. Swartz, "Amplitude compensated horn antennas," *Microwave J.*, vol. 5, pp. 117–122, 1962.
[11] G. Goubau, "Optical and quasi-optical transmission schemes," in *Millimeter and Submillimeter Waves*, F. A. Benson, Ed. London: Iliffe, 1969.
[12] P. F. Goldsmith, "Gaussian beam transformation with cylindrical lenses," *IEEE Trans. Antennas Propagat.*, vol. AP-34, pp. 603–607, 1986.
[13] ——, "Quasi-optical techniques at millimeter and submillimeter wavelengths," in *Infrared and Millimeter Waves*, vol. 6. New York: Academic, 1982, pp. 277–343.

A Systolic Array Architecture for the Applebaum–Howells Array

MOTOHARU UENO, MEMBER, IEEE, K. KAWABATA, MEMBER, IEEE, AND TASUKU MOROOKA, MEMBER, IEEE

Abstract—**A systolic array architecture for the Applebaum–Howells array is derived. A problem to be solved is to eliminate the global signal feedback loop in the conventional Applebaum–Howells array processor. The procedure involved in deriving the architecture consists of two steps: orthogonalization of the input element signals and elimination of the feedback loop. In the first step, the input element signals are orthogonalized with regard to each other by using the Gram–Schmidt processor, placed ahead of the Applebaum–Howells processor. It has been shown, in the second step, that the orthogonality in the Gram–Schmidt processor output signals can remove the global signal feedback loop and that the Applebaum–Howells array can be implemented effectively by using the systolic array with regular structure and local communication. Simulation results also show that the proposed processor features desirable characteristics for the radiation pattern with the low sidelobe level common to the Applebaum–Howells array.**

I. Introduction

Recent sophisticated very large-scale integration (VLSI) technology has led to a new concept in adaptive array antennas, known as the digital beamforming (DBF) concept [1]. In the adaptive array exploiting the DBF concept, array element RF signals are converted into digital video signals and these converted signals are combined in a DBF processor to produce the final array output signal, maximizing a certain operation criterion, such as, for example, the output signal-to-noise ratio. While there are various configurations for the DBF processors, a processor with a regular structure and localized signal transmission paths is required for high-speed operation and easy hardware implementation. A processor architecture, referred to as the systolic array architecture [2], has been developed to satisfy such a requirement. The systolic array architecture consists of unit processors (cells) and has only a unidirectional signal transmission path to the nearest neighbor cells. Consequently, using a DBF processor with a systolic array architecture is considered as the most feasible approach to implement adaptive array processors by using VLSI technology.

Manuscript received December 7, 1988; revised September 5, 1989.
The authors are with Toshiba Research and Development Center, 1, Komukai Toshiba-cho Saiwai-ku, Kawasaki-city 210, Japan.
IEEE Log Number 9036309.

The Gram–Schmidt processor has been investigated for use as a DBF adaptive array processor, and its systolic array structure is well established [3], [4]. A systolic array implementation for adaptive arrays, based on the $Q - R$ decomposition algorithm, has also received attention from many researchers [5], [6]. Although various kinds of systolic array implementation for the adaptive arrays have been proposed, the adaptive arrays having been considered can be essentially categorized into a class of the sidelobe canceller. However, the Applebaum–Howells array [7], a generalized and most important adaptive array, has not been implemented by using the systolic array architecture. This is because the Applebaum–Howells array has a global signal feedback loop configuration where array weight updates are obtained from the correlation between the summed output from the array and signals received by each array element. The difficulty in the hardware configuration for the feedback loop and the resulting time delay due to the loop prevents the array from being used in the systolic array implementation. Indeed, the systolic array implementation problem for the Applebaum–Howells array is a fundamental one to be solved in the adaptive array field.

This communication derives a new systolic array architecture for the Appelbaum–Howells array. The procedure involved in deriving the architecture consists of two steps: orthogonalization of the input element signals and elimination of the feedback loop needed in the conventional Applebaum–Howells array. In the first step, the input element signals are orthogonalized with regard to each other, using the Gram–Schmidt processor placed ahead of the Applebaum–Howells processor. It will be shown, in the second step, that the orthogonality among the Gram–Schmidt processor output signals can remove the global signal feedback loop and that the Applebaum–Howells array can be implemented effectively by using the systolic array architecture.

II. Input Element Signals Orthogonalization

The procedure in the first step is to orthogonalize the input element signals. The preprocessor technique [7] was used for this purpose. Fig. 1(a) shows a typical Applebaum–Howells array, using a preprocessor placed ahead of the Applebaum–Howells processor. In this figure, the Gram–Schmidt processor is assumed to be the preprocessor.

The Gram–Schmidt processor transforms the original signals from the array elements into a new set of signals, which is the signal input to the Applebaum–Howells processor. The input and output relation for the Gram–Schmidt processor is represented by the following matrix notation:

$$v = Qu,$$

where u and v are the input (the original signals from the array elements) and the output (the new set of signals) signal column vectors in the form

$$u = (u_1, u_2, \cdots, u_N)^T,$$

$$v = (v_1, v_2, \cdots, v_N)^T,$$

respectively, and Q is the matrix transforming u into v; superscript T denotes the matrix transpose and N denotes the number of array elements.

As shown in Fig. 1(a), the Gram–Schmidt processor consists of $N - 1$ rows of the unit processors (cells) in the form of a triangle. In the first row of cells, the input signal t_1, letting $t_1 = u$ only for technical reasons, is transformed into the signal t_2. Letting the

0018-926X/90/0800-1310$01.00